INTERNATIONAL JOURNAL OF
NUMERICAL ANALYSIS AND MODELING
Volume 7, Number 3, Pages 462–476

FINITE VOLUME APPROXIMATION OF TWO-DIMENSIONAL STIFF PROBLEMS

CHANG-YEOL JUNG AND ROGER TEMAM

This paper is dedicated to G.I. Shishkin on the occasion of his 70th birthday

Abstract. Continuing an earlier work in space dimension one, the aim of this article is to present, in space dimension two, a novel method to approximate stiff problems using a combination of (relatively easy) analytical methods and finite volume discretization. The stiffness is caused by a small parameter in the equation which introduces ordinary and corner boundary layers along the boundaries of a two-dimensional rectangle domain. Incorporating in the finite volume space the boundary layer correctors, which are explicitly found by analysis, the boundary layer singularities are absorbed and thus uniform meshes can be preferably used. Using the central difference scheme at the volume interfaces, the proposed scheme finally appears to be an efficient second-order accurate one.

Key Words. Finite volume methods, boundary layers, correctors, asymptotic analysis, singularly perturbed problems, stiff problems

1. Introduction

We consider convection-dominated problems in a two-dimensional domain:

$$\begin{cases} div(-\varepsilon\nabla u^\varepsilon - \mathbf{b}u^\varepsilon) = f \text{ in } \Omega, \\ u^\varepsilon = 0 \text{ on } \partial\Omega, \end{cases} \tag{1.1}$$

where $\Omega = (0,1)\times(0,1) \subset \mathbb{R}^2$, $div(\mathbf{b}) = 0$, $\mathbf{b} = (b_1, b_2)^T$ with $b_1, b_2 \geq \delta > 0$ and $\varepsilon > 0$, and $b_1 = b_1(x,y), b_2 = b_2(x,y)$ and $f = f(x,y)$ are sufficiently smooth. When ε is small, e.g. $0 < \varepsilon << \delta$, the solutions u^ε of Problem (1.1) possess boundary layers at the outflow boundaries, that is, $x = 0$, $y = 0$. For the analysis of boundary layers problems the reader is referred to e.g. [4], [5], [8], [9], [11], [21], [23], [25] and [27], and for the numerical approach to e.g. [24], [7], [12], [13], [15] - [19], [22] and [26]. Notice that the boundary $\partial\Omega$ of Ω is nowhere characteristic. Since $div(\mathbf{b}) = 0$, we also note that $div(-\varepsilon\nabla u - \mathbf{b}u) = -\varepsilon\Delta u - \mathbf{b}\cdot\nabla u$ and the well-posedness of Problem (1.1) in the Sobolev space $H_0^1(\Omega)$ is standard, thanks to the Lax-Milgram theorem. Furthermore, we can verify the following norm estimates for the solutions u^ε.

Lemma 1.1. *Let $f = f_1 + f_2 + f_3$. There exists a positive constant κ, independent of ε, such that*

$$\begin{cases} |u^\varepsilon|_{L^2(\Omega)} \leq \kappa N_\varepsilon(f), \\ |u^\varepsilon|_{H^1(\Omega)} \leq \kappa\varepsilon^{-\frac{1}{2}} N_\varepsilon(f), \\ |u^\varepsilon|_{H^2(\Omega)} \leq \kappa\varepsilon^{-\frac{3}{2}} N_\varepsilon(f), \end{cases} \tag{1.2}$$

Received by the editors June 24, 2009 and, in revised form, October 07, 2009.
2000 *Mathematics Subject Classification.* 34D15, 76N20.

where $N_\varepsilon(f) = |f_1|_{L^2(\Omega)} + \varepsilon^{-\frac{1}{2}}|x(L_1-x)f_2|_{L^2(\Omega)} + \varepsilon^{-\frac{1}{2}}|y(L_2-y)f_3|_{L^2(\Omega)}$.

Proof. To estimate $u^\varepsilon = u$, we write $u = e^{-x}v$ and then we have

$$\begin{cases} -\varepsilon\Delta v - div(\mathbf{b}v) + (b_1 - \varepsilon)v + 2\varepsilon v_x = e^x f \text{ in } \Omega, \\ v = 0 \text{ on } \partial\Omega. \end{cases} \tag{1.3}$$

We first observe that

$$-\int_\Omega div(\mathbf{b}v)v = -\int_\Omega (\mathbf{b}\cdot\nabla v)v = \int_\Omega div(\mathbf{b})\frac{v^2}{2} = 0. \tag{1.4}$$

Multiplying then $(1.3)_1$ by v and integrating over Ω, we find

$$\begin{aligned} \varepsilon|v|^2_{H^1} + (\delta-\varepsilon)|v|^2_{L^2} &\le \kappa|x(L_1-x)f_2|_{L^2}|(\frac{1}{x} + \frac{1}{L_1-x})v|_{L^2} \\ &+ \kappa|y(L_2-y)f_3|_{L^2}|(\frac{1}{y} + \frac{1}{L_2-y})v|_{L^2} + \kappa|f_1|_{L^2}|v|_{L^2} \\ &\le \kappa(|f_1|_{L^2}|v|_{L^2} + |x(L_1-x)f_2|_{L^2}|v|_{H^1} + |y(L_2-y)f_3|_{L^2}|v|_{H^1}). \end{aligned} \tag{1.5}$$

In (1.5) we have used the Hardy inequality (see e.g. [19], [10]) in the form:

$$\left|\frac{u}{x}\right|_{L^2(\Omega)} \le \kappa|u|_{H^1(\Omega)}, \text{ for } u = 0 \text{ at } x = 0. \tag{1.6}$$

The first two inequalities (1.2) follow promptly from (1.5). Then the H^2 regularity and the H^2 estimate immediately follow from (1.1). □

Convection-dominated problems appear in many applications where convection plays an important role, as for instance weather-forecasting, oceanography, transport of contaminant, etc. (see e.g. [3]). In this article we build a novel method to approximate, numerically, two-dimensional convection-dominated problems and via numerical examples the new numerical scheme is proved efficient and accurate.

Before we proceed we analyze below the stiffness of the solutions due to the small parameter ε.

2. Singular perturbation analysis

In general, functions like u^ε can be decomposed into a relatively slow (smooth) part u^s and a fast part u^f, i.e. $u^\varepsilon = u^s + u^f$. Using standard classical numerical methods the slow part u^s can be easily approximated, but the fast part u^f produces large approximation errors due to the stiff gradients. Introducing the so-called correctors which appear below we will resolve such issues for the problem under consideration. The singular perturbation analysis provides the two important settings. One is to locate the stiff parts, namely the boundary layers; we will modify them and construct appropriate forms of u^f which absorb the boundary layer singularities. The other is to impose the boundary conditions for the slow parts u^s which are close to the limit solutions.

Writing (1.1) in a non-divergence form we first construct the limit solution of u^ε in (1.1), i.e. when $\varepsilon = 0$. That is, we find

$$\mathbf{b}\cdot\nabla u^0 = f \text{ in } \Omega, \tag{2.1}$$

and then impose the zero boundary conditions at the inflows, i.e. $x = 1$ or $y = 1$. This choice of the boundary condition for (2.1) will be justified a posteriori by our convergence result. The existence and uniqueness of a solution $u^0 \in L^2(\Omega)$ of (2.1) satisfying the zero boundary conditions at the inflows is well-known. In what follows we will assume that u^0 is as regular as needed. Such regularity results may

impose some regularity and compatibility conditions for $\mathbf{b}$ and f, in particular if $\mathbf{b} \cdot n$ vanishes on $\partial\Omega$, where n is the unit outward normal on $\partial\Omega$.

To resolve the mismatch of the boundary values between u^ε and u^0 at the outflows, i.e. $x = 0$ or $y = 0$, we now introduce the so-called ordinary boundary layers θ^1, θ^2 (OBL) in space dimension 1, operating in the direction orthogonal to the boundary. We find these OBL by stretching the space variables respectively near $x = 0$, and $y = 0$, and balancing the dominating differential operators (see e.g. [4] [25], [24], [15]):

$$\begin{cases} -\varepsilon\theta^1_{xx} - b_1(0,y)\theta^1_x = 0 \text{ in } \Omega, \\ \theta^1 = -u^0 \text{ at } x = 0, \\ \theta^1 = 0 \text{ at } x = 1, \end{cases} \tag{2.2}$$

and

$$\begin{cases} -\varepsilon\theta^2_{yy} - b_2(x,0)\theta^2_y = 0 \text{ in } \Omega, \\ \theta^2 = -u^0 \text{ at } y = 0, \\ \theta^2 = 0 \text{ at } y = 1. \end{cases} \tag{2.3}$$

We then see that the asymptotic difference $u^\varepsilon - (u^0 + \theta^1 + \theta^2)$ satisfies the zero boundary condition at $x = 1$, $y = 1$. However, this difference may not be zero at $x = 0$, $y = 0$ due to the correctors θ^1, θ^2 themselves. To resolve this new discrepancy, we introduce the so-called corner boundary layer ξ (CBL) at $(0, 0)$, see e.g. [25]; ξ is the solution of:

$$\begin{cases} -\varepsilon\Delta\xi - b_1(0,0)\xi_x - b_2(0,0)\xi_y = 0 \text{ in } \Omega, \\ \xi = -\theta^2 \text{ at } x = 0,\ \xi = -\theta^1 \text{ at } y = 0, \\ \xi = 0 \text{ at } x = 1, \text{ or } y = 1. \end{cases} \tag{2.4}$$

Finally, the asymptotic difference $w := u^\varepsilon - (u^0 + \theta^1 + \theta^2 + \xi)$ satisfies the zero boundary condition on $\partial\Omega$ and we will now estimate this difference, which measures the asymptotic error. Subtracting $(2.2)_1$, $(2.3)_1$, $(2.4)_1$ from $(1.1)_1$ we obtain

$$\begin{cases} -\varepsilon\Delta w - \mathbf{b} \cdot \nabla w = \varepsilon\Delta u^0 + R_1 + R_2 + R_3 \text{ in } \Omega, \\ w = 0 \text{ on } \partial\Omega, \end{cases} \tag{2.5}$$

where

$$\begin{cases} R_1 = \varepsilon\theta^1_{yy} + b_2(x,y)\theta^1_y + (b_1(x,y) - b_1(0,y))\theta^1_x, \\ R_2 = \varepsilon\theta^2_{xx} + b_1(x,y)\theta^2_x + (b_2(x,y) - b_2(x,0))\theta^2_y, \\ R_3 = (b_1(x,y) - b_1(0,0))\xi_x + (b_2(x,y) - b_2(0,0))\xi_y. \end{cases} \tag{2.6}$$

For the purposes of the following analysis we need explicit expressions of the correctors. Since these explicit expressions are generally not available, we introduce the following approximate forms $\bar\theta^1, \bar\theta^2, \bar\xi$ of the boundary layers θ^1, θ^2, ξ respectively:

$$\begin{cases} \bar\theta^1 = -u^0(0,y)\exp(-b_1(0,y)\dfrac{x}{\varepsilon}), \\ \\ \bar\theta^2 = -u^0(x,0)\exp(-b_2(x,0)\dfrac{y}{\varepsilon}), \\ \\ \bar\xi = u^0(0,0)\exp(-\dfrac{b_1(0,0)x + b_2(0,0)y}{\varepsilon}). \end{cases} \tag{2.7}$$

These approximate forms respectively satisfy the same differential equations with the outflow boundary conditions $(2.2)_{1,2}$, $(2.3)_{1,2}$ and $(2.4)_{1,2}$. But they are *exponentially small terms* (*est*) at the inflow boundaries $x = 1, y = 1$. Hence the differences between the boundary layer functions and their approximate forms satisfy the respective differential equations and are *est* at the boundaries. By standard

a priori estimates, it is thus found that the differences are est too. Denoting by $\bar{R}_1, \bar{R}_2, \bar{R}_3$ the expressions R_1, R_2, R_3 after replacing θ^1, θ^2, ξ by $\bar{\theta}^1, \bar{\theta}^2, \bar{\xi}$, we find:

$$\begin{aligned} |R_1|_{L^2} &\leq \kappa\varepsilon|\bar{\theta}^1_{yy}|_{L^2} + \kappa|\bar{\theta}^1_y|_{L^2} + \kappa|x\bar{\theta}^1_x|_{L^2} + est \\ &\leq \kappa(|\left(\frac{x}{\varepsilon}\right)^2 \bar{\theta}^1|_{L^2} + |\frac{x}{\varepsilon}\bar{\theta}^1|_{L^2}) \leq \kappa|\exp(-c\frac{x}{\varepsilon})|_{L^2} + est \\ &\leq \kappa\varepsilon^{\frac{1}{2}}. \end{aligned} \tag{2.8}$$

We can also estimate $x^n R_1$, for $n \geq 1$:

$$|x^n R_1|_{L^2} \leq \kappa|x^n \exp(-c\frac{x}{\varepsilon})|_{L^2} + est \leq \kappa\varepsilon^{n+\frac{1}{2}}. \tag{2.9}$$

Similarly, we find, for $n \geq 0$,

$$|y^n R_2|_{L^2} \leq \kappa\varepsilon^{n+\frac{1}{2}}. \tag{2.10}$$

For R_3, we obtain that

$$\begin{aligned} |R_3|_{L^2} &\leq |(b_1(x,y) - b_1(0,0))\bar{\xi}_x|_{L^2} + |(b_2(x,y) - b_2(0,0))\bar{\xi}_y|_{L^2} + est \\ &\leq \kappa\varepsilon^{-1}|(x+y)\bar{\xi}|_{L^2} + est \\ &\leq \kappa\varepsilon^{-1}|(x+y)\exp(-b_1(0,y)\frac{x}{\varepsilon})\exp(-b_2(x,0)\frac{y}{\varepsilon})|_{L^2} + est \\ &\leq \kappa\varepsilon. \end{aligned} \tag{2.11}$$

We can also prove that for $n \geq 1$,

$$|x^n R_3|_{L^2} \leq \kappa\varepsilon^{n+1}, \quad |y^n R_3|_{L^2} \leq \kappa\varepsilon^{n+1}. \tag{2.12}$$

Applying Lemma 1.1 to the equation (2.5) with $f_1 = \varepsilon\Delta u^0$, $f_2 = R_1$ and $f_3 = R_2 + R_3$ we can answer at the following result:

Lemma 2.1. *There exists a constant $\kappa > 0$, independent of ε but depending on the other data, such that*

$$\begin{cases} |u^\varepsilon - u^0 - \theta^1 - \theta^2 - \xi|_{L^2} \leq \kappa\varepsilon, \\ |u^\varepsilon - u^0 - \theta^1 - \theta^2 - \xi|_{H^1} \leq \kappa\varepsilon^{\frac{1}{2}}, \\ |u^\varepsilon - u^0 - \theta^1 - \theta^2 - \xi|_{H^2} \leq \kappa\varepsilon^{-\frac{1}{2}}. \end{cases} \tag{2.13}$$

Remark 2.1. From Lemma 2.1 we see that we can decompose u^ε into two parts u^s, u^f in H^1- space. Indeed if we write

$$u^s = w + u^0, \ u^f = \theta^1 + \theta^2 + \xi, \tag{2.14}$$

with $w = w^\varepsilon = u^\varepsilon - u^0 - \theta^1 - \theta^2 - \xi$, (2.13) implies $|w|_{L^2} \leq \kappa\varepsilon$, $|w|_{H^1} \leq \kappa\varepsilon^{\frac{1}{2}}$, so that u^s is indeed smooth (although depending on ε in a "controllable" way). □

In Section 3 the main task will be to approximate the smooth part u^s since u^f is approximated at exponential order by $\bar{\theta}^1 + \bar{\theta}^2 + \bar{\zeta}$ which is explicitly known.

3. The Finite volume schemes

In view of approximating u^s, we now consider a finite volume discretization of the space $H^1_0(\Omega)$. We introduce the mesh or control volumes (cells), nodes (x_i, y_j) and some notations. We first introduce the step functions $\chi_{i,j}$ over the control volumes $K_{i,j}$ where

$$\chi_{i,j} = \chi_{K_{i,j}}(x,y), \ K_{i,j} = (x_{i-\frac{1}{2}}, x_{i+\frac{1}{2}}) \times (y_{j-\frac{1}{2}}, y_{j+\frac{1}{2}}), \tag{3.1}$$

for $i, j = 1, \cdots, N$. For the sake of simplicity, we restrict ourselves to a uniform mesh, so that $x_{i+\frac{1}{2}} - x_{i-\frac{1}{2}} = y_{j+\frac{1}{2}} - y_{j-\frac{1}{2}} = h$. To handle the boundary values on $\partial\Omega$, we consider the fictitious nodes (x_0, y_j), (x_i, y_0), (x_{N+1}, y_j) and (x_i, y_{N+1})

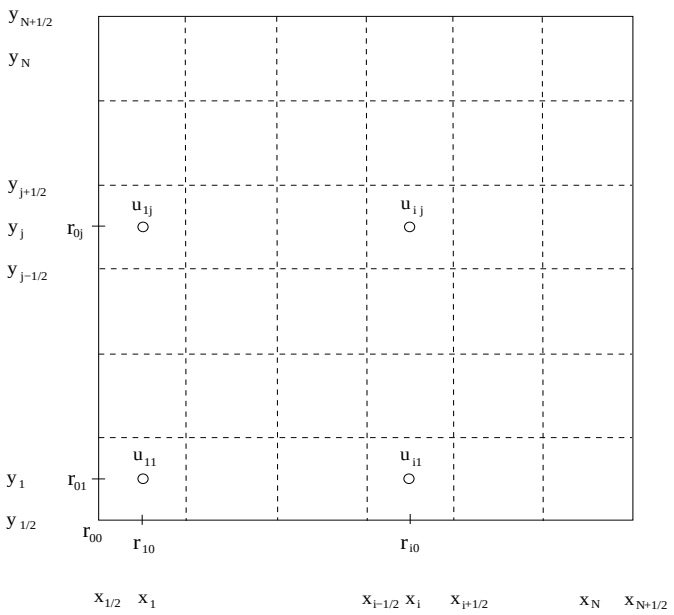

FIGURE 1. Control volumes over 2-dimensional meshes.

for which the nodal values are defined by linear interpolations as we show below. Note then that we can write $x_{i-\frac{1}{2}} = (i-1)h$, $x_i = (i-\frac{1}{2})h$, $y_{j-\frac{1}{2}} = (j-1)h$ and $y_j = (j-\frac{1}{2})h$.

We observe and emphasize the fact that in the proposed method, *we do not need to refine the mesh near the boundary.* In a classic manner (see e.g. [6], [7], [19]), the nodal values $u_{ij} \sim u^s(x_i, y_j)$ are defined at the center of the cells (control volumes) $K_{ij} = (x_{i-\frac{1}{2}}, x_{i+\frac{1}{2}}) \times (y_{j-\frac{1}{2}}, y_{j+\frac{1}{2}})$ (see Figure 1) and the numerical derivatives $\nabla_h u_h$ between the cells are given by

$$\nabla_h^1 u_h = \frac{u_{i+1,j} - u_{ij}}{h} \text{ on } (x_i, x_{i+1}) \times (y_{j-\frac{1}{2}}, y_{j+\frac{1}{2}}), \quad \text{for } i = 1, \cdots, N-1, j = 1, \cdots, N, \tag{3.2a}$$

$$\nabla_h^2 u_h = \frac{u_{i,j+1} - u_{ij}}{h} \text{ on } (x_{i-\frac{1}{2}}, x_{i+\frac{1}{2}}) \times (y_j, y_{j+1}), \quad \text{for } i = 1, \cdots, N, j = 1, \cdots, N-1, \tag{3.2b}$$

where $\nabla_h^1 u_h$ and $\nabla_h^2 u_h$ are respectively the first and second components of $\nabla_h u_h$ and they correspond to approximations of the derivatives of u^s in the x and y directions, respectively. However, since the boundaries are positioned at volume faces (not at nodes), to define $\nabla_h u_h$ on the cells adjacent to the boundaries and to impose the Dirichlet boundary conditions, some specific treatments are necessary, which are the object of Section 3.1.

3.1. Linear interpolation of nodal values at the boundaries. To impose the Dirichlet boundary condition on $\partial\Omega$, we use a linear interpolation between the boundary values of u^s and the nodal values u_{ij} on the cells adjacent to the boundaries $\partial\Omega$. Based on the above singular perturbation analysis and Remark 2.1, since u^s behaves like u^0, we impose the zero boundary conditions for u^s at the inflows $x = 1$, or $y = 1$. At the outflow boundaries $x = 0$, or $y = 0$, we will

cell	$\nabla_h u_h$
$[x_{\frac12}, x_1) \times (y_j, y_{j+\frac12})$	$\left(\frac{2(u_{1j}-r_{0j})}{h}, \frac{u_{1,j+1}-u_{1j}}{h}\right)$
$(x_i, x_{i+\frac12}) \times [y_{\frac12}, y_1)$	$\left(\frac{u_{i+1,1}-u_{i1}}{h}, \frac{2(u_{i1}-r_{i0})}{h}\right)$
$(x_N, x_{N+\frac12}] \times (y_j, y_{j+\frac12})$	$\left(-\frac{2u_{Nj}}{h}, \frac{u_{N,j+1}-u_{Nj}}{h}\right)$
$(x_i, x_{i+\frac12}) \times (y_N, y_{N+\frac12}]$	$\left(\frac{u_{i+1,N}-u_{iN}}{h}, -\frac{2u_{iN}}{h}\right)$

TABLE 1. Numerical derivatives on the cells adjacent to the boundaries; for $i, j = 1, 2, \cdots, N$.

consider the boundary nodal values $r_{0,j}$ at $x = 0$ and $r_{i,0}$ at $y = 0$, for $i, j = 1, \cdots, N$ (see Figure 1). Near the outflows $x = 0$, $y = 0$, to define the numerical derivatives, we approximate the function u^s on the half cells $[x_{\frac12}, x_1) \times (y_{j-\frac12}, y_{j+\frac12})$, $(x_{i-\frac12}, x_{i+\frac12}) \times [y_{\frac12}, y_1)$, $(x_N, x_{N+\frac12}] \times (y_{j-\frac12}, y_{j+\frac12})$, and $(x_{i-\frac12}, x_{i+\frac12}) \times (y_N, y_{N+\frac12}]$, $i, j = 0, 1, 2, \cdots, N$, respectively, by linear functions $z_i = z_i(x, y)$, $i = 1, 2, 3, 4$,

$$z_1 = \frac{2(u_{1j} - r_{0j})x}{h} + r_{0j}, \qquad z_2 = \frac{2(u_{i1} - r_{i0})y}{h} + r_{i0}, \tag{3.3a}$$

$$z_3 = \frac{2u_{Nj}(1-x)}{h}, \qquad z_4 = \frac{2u_{iN}(1-y)}{h}. \tag{3.3b}$$

Differentiating $z_i(x, y)$ the numerical derivatives for u_x and u_y on these half cells are thus obtained. Here we use the interpolations: on the cell $[x_{\frac12}, x_1) \times (y_j, y_{j+\frac12})$, e.g.

$$\nabla_h^1 u_h = \frac{u_{1,j} - u_{0j}}{h} = \frac{u_{1,j} - z_1(-\frac{h}{2}, y_j)}{h} = \frac{2(u_{1j} - r_{0j})}{h}. \tag{3.4}$$

The numerical derivatives on such cells can then be evaluated in a similar manner as in Table 1.

The cell K_{11} near the corner $(0, 0)$ is divided into two triangular cells which are separated by the line $y = x$. Let us call the upper triangular cell U_{11} and the lower one L_{11}. We then approximate u^s on each triangular cell by linear functions $z_5 = z_5(x, y)$ and $z_6 = z_6(x, y)$ which resp. pass through r_{00}, r_{10} and u_{11} and r_{00}, r_{01} and u_{11} where r_{00} is the nodal value at $(0, 0)$:

$$\begin{aligned} z_5 &= u_{11} + \frac{2}{h}\Big[(u_{11} - r_{01})(x - \frac{h}{2}) + (r_{01} - r_{00})(y - \frac{h}{2})\Big], \\ z_6 &= u_{11} + \frac{2}{h}\Big[(r_{10} - r_{00})(x - \frac{h}{2}) + (u_{11} - r_{10})(y - \frac{h}{2})\Big]. \end{aligned} \tag{3.5}$$

Differentiating z_5, z_6 we obtain the numerical derivatives on the triangular cells U_{11}, L_{11} as in Table 2.

3.2. Classical finite volume schemes. Multiplying $(1.1)_1$ by a step function $\chi_{i,j}$, integrating over Ω and applying the divergence theorem we find:

$$-\varepsilon \int_{\partial K_{ij}} \frac{\partial u}{\partial \nu} - \int_{\partial K_{ij}} u\mathbf{b} \cdot \nu = \int_{K_{ij}} f. \tag{3.6}$$

We write $F_{i,j} = f_{ij} vol(K_{ij}) = f_{ij} h^2$ and use the central differencing (CD) for the convective term $u\mathbf{b}$, that is, e.g. at the volume faces $(x_{i+\frac12}, y_j)$, we take the average

cell	$\nabla_h u_h$
U_{11}	$\left(\frac{2(u_{11}-r_{01})}{h}, \frac{2(r_{01}-r_{00})}{h}\right)$
L_{11}	$\left(\frac{2(r_{10}-r_{00})}{h}, \frac{2(u_{11}-r_{10})}{h}\right)$

TABLE 2. Numerical derivatives on the triangular cells adjacent to the corner $(0,0)$.

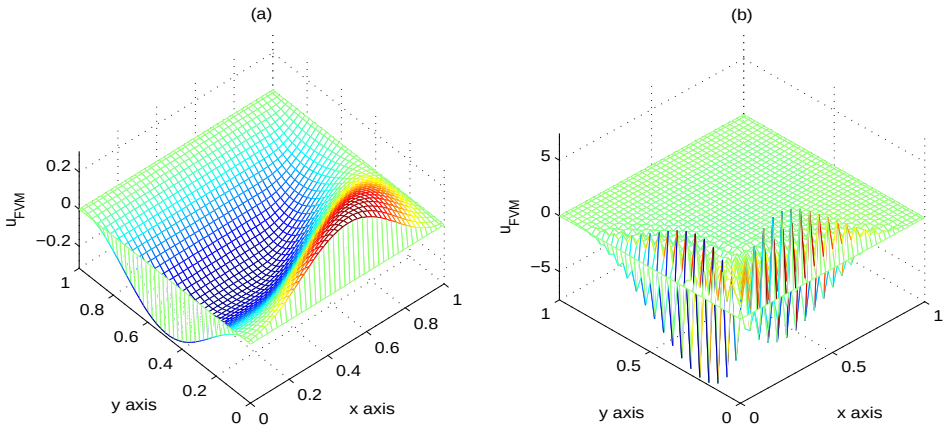

FIGURE 2. Numerical solutions for $-\varepsilon\Delta u^\varepsilon - u^\varepsilon_x - u^\varepsilon_y = \sin(2\pi y)$ with $\varepsilon = 10^{-3}$, $N = 40$, and the Dirichlet boundary conditions $u^\varepsilon = 0$ on $\partial\Omega$: (a) solution using the New finite volume methods (3.19) with the correctors $\theta_w, \theta_s, \theta_o$ (nFVM); (b) solution using the Classical finite volume methods (3.7) without the correctors (cFVMCD).

of two nodal values respectively at (x_i, y_j), (x_{i+1}, y_j)), namely $(\mathbf{b}u)(x_{i+\frac{1}{2}}, y_j) = \frac{1}{2}((\mathbf{b}u)(x_i, y_j) + (\mathbf{b}u)(x_{i+1}, y_j))$. Replacing u by $u_h = \sum_{i,j\geq 1} u_{i,j}\chi_{i,j}$ and $\partial u/\partial\nu$ by $\nu \cdot \nabla_h u_h$ as above we obtain the discrete system corresponding to the equation (3.6): for $i, j = 1, \cdots, N$,

$$
\begin{aligned}
&(-\varepsilon + b_{1,i-1,j}\frac{h}{2})u_{i-1,j} + (-\varepsilon + b_{2,i,j-1}\frac{h}{2})u_{i,j-1} + 4\varepsilon u_{i,j} \\
&\quad + (-\varepsilon - b_{2,i,j+1}\frac{h}{2})u_{i,j+1} + (-\varepsilon - b_{1,i+1,j}\frac{h}{2})u_{i+1,j} = F_{i,j},
\end{aligned} \tag{3.7}
$$

where $(b_{1,i,j}, b_{2,i,j}) = (b_1(x_i, y_j), b_2(x_i, y_j))$. *Note that our method allows us to use here the central differencing, which is second-order accurate whereas the upwind differencing, usually used, which takes upstream nodes at the volume faces, is only first-order accurate* (see [19], [28]).

As usual, we simply impose the zero boundary conditions $(1.1)_2$ by setting $r_{0j} = r_{i0} = 0$ at the outflow beside the zero inflow boundary conditions. For this, from the linear interpolations (3.3) we consider the fictitious points outside the domains which will be incorporated in the scheme (3.7), i.e. with $r_{0j} = r_{i0} = 0$,

$$u_{0j} = z_1(-\frac{h}{2}, y_j) = -u_{1j}, \qquad u_{i0} = z_2(x_i, -\frac{h}{2}) = -u_{i1}, \tag{3.8a}$$

$$u_{N+1,j} = z_3(1+\frac{h}{2}, y_j) = -u_{N,j}, \qquad u_{i,N+1} = z_4(x_i, 1+\frac{h}{2}) = -u_{i,N}. \tag{3.8b}$$

The scheme (3.7) then corresponds to the following variational problem:
To find $u_h \in V_h$ such that

$$a_h(u_h, v_h) \ = < f, v_h >, \ \forall \ v_h = \sum_{k=0}^{N+1}\sum_{l=0}^{N+1} u_{k,l}\chi_{k,l} \in V_h, \tag{3.9}$$

where $a_h(u_h, v_h) = \sum_{k,l} v_{k,l} \int_{\partial K_{kl}} (-\varepsilon \partial u_h/\partial \nu - u_h \mathbf{b}\cdot\nu)$ and

$$V_h = \Big\{ span\{\chi_{k,l}\}_{k,l=0,1,\cdots,N,N+1} \text{ with the conditions (3.8)} \Big\}. \tag{3.10}$$

However, when ε is small, the classical schemes (3.7) with (3.8) cannot capture the boundary layer singularities and then the large approximation errors due to them propagate along the characteristics. This makes the scheme highly unstable (see [19] and Figure 2 below).

To resolve such issues, we show in the following sections how to capture the boundary singularities by enriching the spaces V_h with the correctors.

3.3. Corrector basis. We now consider the new schemes which incorporate the correctors' basis to absorb the stiffness of the solutions. Based on the above singular perturbation theory and Remark 2.1, we infer that the stiffness is attributed to the boundary layers at the outflows, i.e. θ^1, θ^2, ξ. We approximate the fast part u^f using the functions $e^{-\frac{b_1(0,0)x + b_2(0,0)y}{\varepsilon}}$, $-e^{-\frac{b_1(0,y_j)x}{\varepsilon}}$ and $-e^{-\frac{b_2(x_i,0)y}{\varepsilon}}$ and the slow part u^s by usual classical elements $\sum_{i,j\geq 1} u_{i,j}\chi_{i,j}$. We write the corrector basis, θ_w, θ_s and θ_o,

$$\begin{cases} \theta_w = \theta_w(x) = -\exp(-b_1(0,y_j)\dfrac{x}{\varepsilon}), \text{for } j = 1, \cdots, N, \\ \\ \theta_s = \theta_s(y) = -\exp(-b_2(x_i,0)\dfrac{y}{\varepsilon}), \text{for } i = 1, \cdots, N, \\ \\ \theta_o = \theta_o(x,y) = \exp(-\dfrac{b_1(0,0)x + b_2(0,0)y}{\varepsilon}), \text{for } i = j = 1, \end{cases} \tag{3.11}$$

and assuming that the thickness of the boundary layers is concentrated within one mesh (that is $\varepsilon << h$) we may consider the corrector basis supported in one mesh, i.e. e.g. $\theta_w = \theta_w(x)\chi_{[0,h]}(x)$. We introduce a usual finite volume space V_h, i.e. step functions as above, and add to it the functions, $\theta_w \chi_{(0,h)\times(y_{j-\frac{1}{2}}, y_{j+\frac{1}{2}})}$, $\theta_s \chi_{(x_{i-\frac{1}{2}}, x_{i+\frac{1}{2}})\times(0,h)}$ and $\theta_o \chi_{(0,h)\times(0,h)}$ corresponding to $\bar{\theta}^1$, $\bar{\theta}^2$, $\bar{\xi}$, and we obtain the *enriched finite volume spaces*. In the enriched FV space we then approximate the solution u^ε of (1.1) by $\tilde{u}_h$

$$\tilde{u}_h = r_{00}\theta_o\chi_{0,0} + \sum_{j=1}^{N} r_{0,j}\theta_w\chi_{0,j} + \sum_{i=1}^{N} r_{i,0}\theta_s\chi_{i,0} + \sum_{i,j\geq 0} u_{i,j}\chi_{i,j}, \tag{3.12}$$

where, $\chi_{0,0} = \chi_{(0,h)\times(0,h)}$, $\chi_{0,j} = \chi_{(0,h)\times(y_{j-\frac{1}{2}},y_{j+\frac{1}{2}})}$, $\chi_{i,0} = \chi_{(x_{i-\frac{1}{2}},x_{i+\frac{1}{2}})\times(0,h)}$, and the $\chi_{i,j}$, for $i,j \geq 1$, are as in (3.1).

The derivative ∇u^ε is then approximated by a numerical derivative $\nabla_h \tilde{u}_h$ (see e.g. [19])

$$\nabla_h \tilde{u}_h = r_{00}\nabla\theta_o\chi_{0,0} + \sum_{j=1}^{N} r_{0,j}\nabla\theta_w\chi_{0,j} + \sum_{i=1}^{N} r_{i,0}\nabla\theta_s\chi_{i,0} + \nabla_h u_h, \tag{3.13}$$

where $\nabla_h u_h$ is defined in (3.2) and in the Tables 1, 2.

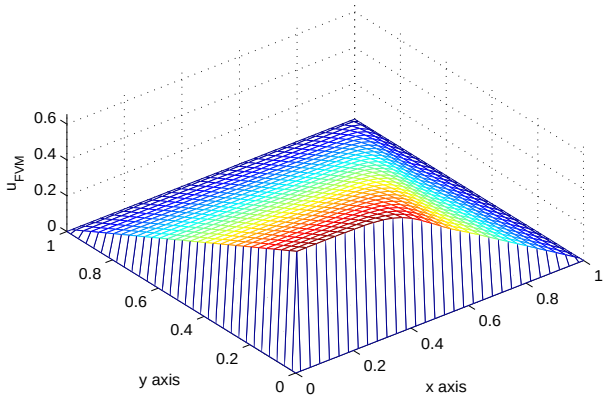

FIGURE 3. Numerical solutions for $-\varepsilon\Delta u^\varepsilon - u^\varepsilon_x - 1.5u^\varepsilon_y = 1$ with $\varepsilon = 10^{-3}$, $N = 30$, and the Dirichlet boundary conditions $u^\varepsilon = 0$ on $\partial\Omega$ using the New finite volume methods (3.19) with the correctors $\theta_w, \theta_s, \theta_o$ (nFVM).

3.4. The new finite volume schemes. In the new schemes, we assume that the r_{0j}, and r_{i0} (see Figure 1) are free at the outflow and set the nodal values equal to zero at the inflow boundaries. From the linear interpolations (3.3) we can, as in (3.8), define the values of u^s at the fictitious nodes:

$$u_{0j} = 2r_{0j} - u_{1j}, \qquad u_{i0} = 2r_{i0} - u_{i1}, \tag{3.14a}$$

$$u_{N+1,j} = -u_{N,j}, \qquad u_{i,N+1} = -u_{i,N}. \tag{3.14b}$$

Hence we can setup the scheme (3.7) with the nodal values as in (3.14). However, due to the nodes $r_{0,j}$, $r_{i,0}$, the system for this scheme is not closed. But it can be closed using the correctors $\theta_w\chi_{0,j}, \theta_s\chi_{i,0}, \theta_o$ as test elements as we will show below.

We start with the generic test elements $\chi_{i,j}$. For $1 \leq i,j \leq N$, multiplying $(1.1)_1$ by $\chi_{i,j}$, integrating over Ω and replacing u^ε by $\tilde{u}_h$ as in (3.12) we find that the equations are equivalent to those of the classical FV scheme (3.7). *Note that the correctors $\theta_w, \theta_s, \theta_o$ (and similarly below) do not contribute to these equations because the correctors are the solutions of (1.1) with $f = 0$.*

Multiplying $(1.1)_1$ by $\theta_w(x)\chi_{1,j}$, $j = 1, 2, \cdots, N$ and integrating over Ω we first find that

$$-\int_{\partial K_{1,j}} \varepsilon \frac{\partial u}{\partial \nu}\theta_w + \int_{K_{1,j}} (\varepsilon u_x \theta_{wx} - (\mathbf{b}\cdot\nabla u)\theta_w) = \int_{K_{1,j}} f\theta_w. \tag{3.15}$$

Since $\theta_{wx} = -b_{1,\frac{1}{2},1}\varepsilon^{-1}\theta_w$, we can rewrite (3.15) as

$$-\int_{\partial K_{1,j}} \varepsilon \frac{\partial u}{\partial \nu}\theta_w - \int_{K_{1,j}} ((b_{1,\frac{1}{2},1} + b_{1,1,1}, b_{2,1,\frac{1}{2}})\cdot\nabla u)\theta_w = \int_{K_{1,j}} f\theta_w. \tag{3.16}$$

Note that $\int_{K_{k,l}} f = O(h^2)$ for $i, j \geq 1$, but $\int_{K_{1,j}} f\theta_w = O(h\varepsilon)$, for $j \geq 1$. To balance this equation with the other equations in (3.19) below, we will multiply (3.16) by h/ε.

We can similarly derive an equation associated to the test function $\theta_s(y)\chi_{i,1}$. We just switch the roles of x and y, and of b_1 and b_2.

For $i = j = 1$, multiplying $(1.1)_1$ by $\theta_o(x, y)\chi_{1,1}$ and integrating over Ω we find that

$$-\int_{\partial K_{1,1}} \varepsilon \frac{\partial u}{\partial \nu}\theta_o + \int_{K_{1,1}} (\varepsilon \nabla u\cdot\nabla\theta_o - (\mathbf{b}\cdot\nabla u)\theta_o) = \int_{K_{1,1}} f\theta_o. \tag{3.17}$$

Since $\nabla\theta_o = (-b_{1,\frac{1}{2},1}, -b_{2,1,\frac{1}{2}})\varepsilon^{-1}\theta_0$, we can rewrite this as

$$-\int_{\partial K_{1,1}} \varepsilon \frac{\partial u}{\partial \nu}\theta_o - \int_{K_{1,1}} ((b_{1,\frac{1}{2},1} + b_{1,1,1}, b_{2,1,\frac{1}{2}} + b_{2,1,1})\cdot\nabla u)\theta_o = \int_{K_{1,1}} f\theta_o. \tag{3.18}$$

We note that $\int_{K_{1,1}} f\theta_o = O(\varepsilon^2)$. To balance this equation with the other equations, we will multiply it by h^2/ε^2.

Replacing the derivatives $\partial u/\partial\nu$ and ∇u as in (3.16) and (3.18) by the numerical derivatives $\nu\cdot\nabla_h\tilde{u}_h$ and $\nabla_h\tilde{u}_h$ as in (3.13) and combining the classical equations (3.7) with (3.14) we obtain the following new scheme: for $i, j = 0, 1, \cdots, N$,

(3.19a)

$$\begin{cases} \text{for } i = j = 0, \\ (4b_{2,1,\frac{1}{2}}C + 4b_{1,\frac{1}{2},1}D)hr_{0,0} + (-2\dfrac{1-A_2}{b_{2,1,\frac{1}{2}}} + (4b_{1,\frac{1}{2},1} - 4b_{2,1,\frac{1}{2}})C)hr_{0,1} \\ \quad +(-2\dfrac{1-B_2}{b_{1,\frac{1}{2},1}} - (4b_{1,\frac{1}{2},1} - 4b_{2,1,\frac{1}{2}})D)hr_{1,0} \\ \quad +(\dfrac{(2+B_2)(1-A_2)}{b_{2,1,\frac{1}{2}}} + \dfrac{(2+A_2)(1-B_2)}{b_{1,\frac{1}{2},1}} - 4b_{1,\frac{1}{2},1}C - 4b_{2,1,\frac{1}{2}}D)hu_{1,1} \\ \quad -\dfrac{A_2(1-B_2)}{b_{1,\frac{1}{2}},1}hu_{1,2} - \dfrac{B_2(1-A_2)}{b_{2,1,\frac{1}{2}}}hu_{2,1} = F_{0,0}, \end{cases}$$

(3.19b)

$$\begin{cases} \text{for } i=0,\ j\geq 1, \\ (2-4B_1)hr_{0,j}+(-2h+6hB_1-hB_2+2\varepsilon\dfrac{1-B_2}{b_{1,\frac12,1}})u_{1,j}+(-2B_1+B_2)hu_{2,j} \\ \quad -\dfrac{2\varepsilon+b_{2,1,\frac12}h}{2b_{1,\frac12,1}}(1-B_2)u_{1,j+1}-\dfrac{2\varepsilon-b_{2,1,\frac12}h}{2b_{1,\frac12,1}}(1-B_2)u_{1,j-1}=F_{0,j}, \\ \\ \text{for } i\geq 1,\ j=0, \\ (2-4A_1)hr_{i,0}+(-2h+6hA_1-hA_2+2\varepsilon\dfrac{1-A_2}{b_{2,1,\frac12}})u_{i,1}+(-2A_1+A_2)hu_{i,2} \\ \quad -\dfrac{2\varepsilon+b_{1,\frac12,1}h}{2b_{2,1,\frac12}}(1-A_2)u_{i+1,1}-\dfrac{2\varepsilon-b_{1,\frac12,1}h}{2b_{2,1,\frac12}}(1-A_2)u_{i-1,1}=F_{i,0}, \end{cases}$$

(3.19c)

$$\begin{cases} \text{for } i,j\geq 1, \\ (-\varepsilon+b_{1,i-1,j}\dfrac{h}{2})u_{i-1,j}+(-\varepsilon+b_{2,i,j-1}\dfrac{h}{2})u_{i,j-1}+4\varepsilon u_{i,j} \\ \quad +(-\varepsilon-b_{2,i,j+1}\dfrac{h}{2})u_{i,j+1}+(-\varepsilon-b_{1,i+1,j}\dfrac{h}{2})u_{i+1,j}=F_{i,j}. \end{cases}$$

In (3.19) we have set, for $k=1,2$:

(3.20)

$$\begin{cases} A_k=\exp(-b_{2,1,\frac12}\dfrac{kh}{2\varepsilon}),\ B_k=\exp(-b_{1,\frac12,1}\dfrac{kh}{2\varepsilon}), \\ \\ C=\dfrac{A_2B_2-1}{b_{1,\frac12,1}(b_{1,\frac12,1}+b_{2,1,\frac12})}-\dfrac{A_2-1}{b_{1,\frac12,1}b_{2,1,\frac12}}, \\ \\ D=\dfrac{A_2B_2-1}{b_{2,1,\frac12}(b_{1,\frac12,1}+b_{2,1,\frac12})}-\dfrac{B_2-1}{b_{1,\frac12,1}b_{2,1,\frac12}}, \end{cases}$$

(3.21) $$F_{11}=\frac{h^2}{\varepsilon^2}\int_{K_{1,1}} f\theta_o,\ F_{0j}=\frac{h}{\varepsilon}\int_{K_{1,j}} f\theta_w,\ F_{i0}=\frac{h}{\varepsilon}\int_{K_{i,1}} f\theta_s,\ F_{ij}=\int_{K_{i,j}} f,$$

and the fictitious nodes $u_{0j}, u_{i0}, u_{N+1,j}, u_{i,N+1}$ are as in the relations (3.14).

Remark 3.1. In (3.15) (similarly in (3.17)) rather than a divergence form we use a non-divergence form of Eq. (1.1). The reason is due to discretization errors. More precisely, if we use a divergence form, the term $\int_{K_{1,j}}(\mathbf{b}\cdot\nabla u)\theta_w$ in (3.15) can be written as $\int_{K_{1,j}} ub_1\theta_{wx}$ and we then find the discretization error $\int_{K_{1,j}}(ub_1(x)-u_hb_{1,1,1})\theta_{wx}=\mathcal{O}(h\epsilon^{-\frac12})$, which is getting large as ϵ is getting small. This error can lead to a instability of numerical schemes. However, the discretization error due to the term $\int_{K_{1,j}}(\mathbf{b}\cdot\nabla u)\theta_w$ is only $\mathcal{O}(h)$.

4. Numerical examples

To test the numerical accuracy of the classical and new finite volume schemes, an analytic explicit solution with a given boundary condition is usually suggested. But it is difficult to have an explicit solution u^ε of Eq. (1.1) (with sharp boundary layers) if f does not have singular terms of the type $e^{-x/\varepsilon}$. Hence, for comparison purpose, we take $f=-2x+2$, $b_1=b_2=1$ and the boundary conditions $u^\varepsilon=0$ at $x=0,1$ and assume periodicity with period 1 in the y direction. Since we expect boundary layers at $x=0$ only, for the new schemes (3.19), we set $r_{i,0}=0$ for $i\geq 0$ and we thus remove the first and the third equations of (3.19) and thanks to the

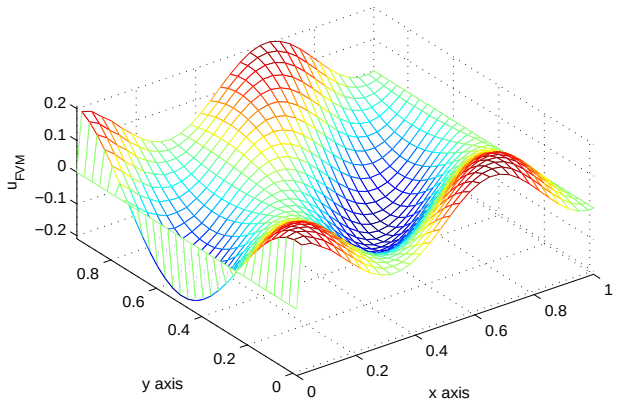

FIGURE 4. Numerical solutions for $-\varepsilon\Delta u^\varepsilon - u^\varepsilon_x - 1.5u^\varepsilon_y = \sin(2\pi y)$ with $\varepsilon = 10^{-3}$, $N = 30$, and the boundary conditions $u^\varepsilon = 0$ at $x = 0, 1$ and 1- periodic in y using the New finite volume methods (3.19) with the corrector θ_w only (nFVM).

periodicity in y replace the second and the last relation of the fictitious nodes in (3.14) by $u_{i,0} = u_{i,N}$, $u_{i,N+1} = u_{i,1}$ respectively. Similarly, for the classical schemes (3.7), we use these two relations to replace the second and the last ones in (3.8). The exact solution is easily found:

$$u^\varepsilon = (1 - e^{-\frac{1}{\varepsilon}})^{-1}(e^{-\frac{1}{\varepsilon}} + 2\varepsilon - (1 + 2\varepsilon)e^{-\frac{x}{\varepsilon}}) + x^2 - 2(1 + \varepsilon)x + 1. \tag{4.1}$$

As it appears in Table 3, the new finite volume methods (nFVM) (3.19) attain much better numerical accuracy for $\varepsilon \leq 10^{-1}$ whereas the classical finite volume methods with center differencing (cFVMCD) (3.7) do so for $\varepsilon = 1$ (ε *not small*) but, as $\varepsilon \to 0$, the cFVMCD becomes highly unstable and with upwind differencing (cFVMUD) the classical scheme is stable but less accurate than the nFVM. In Figure 4 imposing the same boundary conditions with $f = \sin(2\pi y)$ we can also obtain stable and accurate numerical solutions. In this case, we expect the boundary layers to occur at $x = 0$ and incorporate the corrector θ_w.

In Figure 2 we compare the simulations for the new and the classical schemes. Firstly, we easily see that the numerical errors from the classical schemes cFVMCD propagate along the characteristics, $y = x + c$, c constants. More precisely, the large approximation errors due to the stiffness of the boundary layers at $x = 0$, or $y = 0$ propagate in the convective directions. To capture the stiffness, highly fine meshes are needed when using the classical finite volume schemes. On the contrary, the numerical solutions obtained with the new schemes nFVM are stable and capture the boundary layers at $x = 0$, and $y = 0$ with economical mesh sizes.

In Figure 3 we clearly observe the boundary layers at $x = 0$, $y = 0$ and the characteristics are $y = 1.5x + c$, c constants, and the new schemes capture all the boundary layers.

ε	N	nFVM	cFVMCD	cFVMUD
1	10	8.3570E-01	3.2196E-03	3.9710E-03
1	20	8.5300E-01	8.3143E-04	2.4769E-03
1	40	8.6200E-01	2.1119E-04	1.3687E-03
10^{-1}	10	2.5535E-03	1.2533E-01	8.2272E-02
10^{-1}	20	6.7887E-04	3.3935E-02	5.7310E-02
10^{-1}	40	2.1021E-04	8.8401E-03	3.4563E-02
10^{-3}	10	2.6856E-03	1.5094E+02	8.2286E-02
10^{-3}	20	7.1281E-04	3.0378E+01	4.4832E-02
10^{-3}	40	1.9543E-04	1.1543E+01	5.1539E-02
10^{-8}	10	2.5000E-03	1.2499E+12	9.2500E-02
10^{-8}	20	6.2500E-04	1.5625E+11	4.8125E-02
10^{-8}	40	1.5625E-04	1.9532E+10	2.4530E-02

TABLE 3. The numerical accuracies, measured by the max norm, $\max_{1\le i,j\le N}\{|u(x_i,y_j)-u_{ij}|\}$ where $u(x_i,y_j)$ are exact solutions from (4.1) and u_j are numerical solutions from the classical finite volume methods (3.7) with central differencing (cFVMCD), upwind differencing (cFVMUD), and new finite volume methods (nFVM) (3.19) where $-\varepsilon\Delta u^\varepsilon - u^\varepsilon_x - u^\varepsilon_y = -2x+2$ with the boundary conditions $u^\varepsilon = 0$ at $x = 0, 1$ and 1- periodic in y.

5. Conclusion

We have extended to 2D problems our approach developed in ([19]) for one-dimensional problems, where we verified the stability and convergence analysis. In the 1D problem we have only one ordinary boundary layer at the outflow whereas in the 2D problem under consideration we observe, beside the boundary layers along the outflow boundaries, the corner boundary layers located at the corner where the two boundary layers intersect. Incorporating into the FV space the correctors $\theta_w, \theta_s, \theta_o$, which absorb the singularities of the ordinary and corner boundary layers, and using the central differencing (CD) we are able to achieve the second-order numerical accuracy in the Taylor series truncation error (see Table 3 and see the truncation error analysis in [19]). Furthermore, since the boundary layer singularities are absorbed by the correctors, we are able to use a uniform mesh. The new finite volume scheme (3.19) is thus efficient (compared to the use of meshes refined near the boundary layers), stable and second-order accurate. Here we note that the upwind differencing (UP) which is standard in classical schemes is only first-order accurate in the truncation error.

It is noteworthy to estimate the mesh size h that is needed if the boundary layer singularities are not appropriately absorbed as we do. For simplicity, let us consider the one-dimensional version of the problem under consideration. The interpolation errors for u^ε near $x = 0$ (say over a mesh $[x_i, x_{i+1}]$) in e.g. the H^1- space are bounded from above by $\kappa h|u^\varepsilon|_{H^2(x_i,x_{i+1})}$ (see [19]). By asymptotic analysis, it is not difficult to estimate u^ε as $u^\varepsilon \sim e^{-cx_i/\varepsilon}$ and $|u^\varepsilon|_{H^2(x_i,x_{i+1})} \sim \varepsilon^{-3/2}e^{-cx_i/\varepsilon}$, $c > 0$, near the boundary. Hence, to guarantee that $|u^\varepsilon|_{H^2(x_i,x_{i+1})} \le \kappa$, we must require the mesh points x_i to be $x_i \sim -\frac{3}{2}\varepsilon \ln \varepsilon$ which indicates extremely small meshes as $\varepsilon \to 0$. Our scheme, which absorbs the boundary singularities in the corrector, only

requires uniform meshes and is definitely much more efficient. We plan, in a future more experimental work, to compare e.g. the CPU times required by the different modes, but we see already that our method avoids refining the mesh (too often) as $\varepsilon \to 0$.

We have used the central differencing at the volume interfaces. Absorbing the singularities due to boundary layers the numerical stability is already achieved (very robust with respect to changes of ε) and thus usual higher-order techniques can be implemented such as the stability preserving higher-order methods, e.g. central upwind, MUSCL, which appear in classical finite volume or discontinuous Galerkin methods. Note however that the numerical solutions of the stability preserving higher-order methods are known to be smearing (or to have relatively low numerical accuracies) near the boundary layers.

We may extend our method to more complex problems. Without any changes taking the tensor product of 1D finite volume spaces we can easily apply to 3D version of (1.1) on a cubic domain as we did the 2D version (1.1) from the 1D problem in [19]. On curvilinear domains when $\mathbf{b} \cdot \nu$ does not change sign on $\partial\Omega$, since the boundary layer correctors are 1-dimensional (see [9], [8]), we can also obtain explicit forms of the correctors and incorporate them in the FV spaces. We may also consider more general elliptic operators of second or higher order, or time dependant problems (see [14], [3], [20], [1], [2]). In the case where the convective coefficients $\mathbf{b} \cdot \nu$ change sign, the difficulties are considerable due to the turning point layers (see e.g [18] for 1D problems). In general the curves where the turning points occur are complex and the turning point layer correctors should be modified and simplified to be used in the discretizations. We will extend our method to resolve such issue as well as problems on 3D domains, curvilinear domains, and turning point layers in the future.

Acknowledgments

This work was supported in part by NSF Grant DMS 0906440, and by the Research Fund of Indiana University and by Basic Science Research Program through the National Research Foundation of Korea(NRF) funded by the Ministry of Education, Science and Technology (20100015696)

References

[1] B. Cockburn, F. Coquel and P. G. LeFloch, *Convergence of the finite volume method for multidimensional conservation laws.* SIAM J. Numer. Anal. 32 (1995), no. 3, pp 687-705.

[2] B. Cockburn, G. Kanschat and D. Schotzau, *A locally conservative LDG method for the incompressible Navier-Stokes equations.* Math. Comp. 74 (2005), no. 251, pp 1067-1095

[3] B. Cockburn and C.-W. Shu, *Runge-Kutta Discontinuous Galerkin Methods for Convection-Dominated Problems.* J. of Sci. computing, 16 (2001), pp 173 - 261.

[4] W. Eckhaus, *Boundary layers in linear elliptic singular perturbations.* SIAM Rev., **V. 14** (1972), pp. 225-270.

[5] W. Eckhaus and E. M. De Jager, *Asymptotic Solutions of Singular Perturbation Problems for Linear Differential Equations of Elliptic Type.* Arch. Rational Mech. Anal., **V. 23** (1966), pp. 26-86.

[6] R. Eymard, T. Gallouet and R. Herbin, *Finite volume methods*, Handbook of Numerical Analysis vol. VII, North-Holland (2000), pp. 713-1020.

[7] S. Faure, D. Pham and R. Temam *Comparison of finite voulume and finite difference methods and applications.* Analysis and applications. V. 4 (2006), no. 2, pp 163-208.

[8] G. Gie, *Singular perturbation problems in a general smooth domain*, Asymptotic Analysis, vol. 62, no. 3-4, 2009, 227-249.

[9] G. Gie, M. Hamouda and R. Temam, *Boundary layers in smooth curvilinear domains: Parabolic problems*, Discrete and Continuous Dynamical Systems - Series A, 2009, to appear.

[10] M. Hamouda, C. Jung and R. Temam, *Boundary layers for the 2D linearized primitive equations.* Communication on Pure and Applied Analysis, v. 8, no. 1 (2009), pp 335-359
[11] H. Han and R.B. Kellogg, *A method of enriched subspaces for the numerical solution of a parabolic singular perturbation problem.* Computational and asymptotic methods for boundary and interior layers (Dublin, 1982), pp 46–52
[12] C. Jung, *Numerical approximation of two-dimensional convection-diffusion equations with boundary layers*. Numer. Methods Partial Differential Equations, 21(2005), pp. 623-648.
[13] C. Jung, *Finite elements scheme in enriched subspaces for singularly perturbed reaction-diffusion problems on a square domain*. Asymptotic Analysis, v.57 (2008), pp 41-69.
[14] C. Jung, M. Petcu and R. Temam, *Singular perturbation analysis on a homogeneous ocean circulation model*. In preparation.
[15] C. Jung and R. Temam, *Numerical approximation of two-dimensional convection-diffusion equations with multiple boundary layers*. Internat. J. Numer. Analysis and Modeling. 2(2005), pp 367-408.
[16] C. Jung and R. Temam, *On parabolic boundary layers for convection-diffusion equations in a channel: Analysis and Numerical applications*. J. Sci. Comput. 28 (2006), pp 361-410.
[17] C. Jung and R. Temam, *Construction of boundary layer elements for singularly perturbed convection-diffusion equations and L^2- stability analysis.* International Journal of Numerical Analysis and Modeling, 5(2008), no. 4, pp 729 - 748.
[18] C. Jung and R. Temam, *Asymptotic analysis for singularly perturbed convection-diffusion equations with a turning point*. Journal of Mathematical Physics, v. 48, no.6, 065301(2007) (27 pages)
[19] C. Jung and R. Temam, *Finite volume approximation of one-dimensional stiff reaction-convection equations.* To appear in Journal of scientific computing.
[20] R. B. Kellogg and M. Stynes, *Layers and corner singularities in singularly perturbed elliptic problems.* BIT 48 (2008), no. 2, pp 309 -314.
[21] J. L. Lions, Perturbations singulières dans les problèmes aux limites et en contrôle optimal. (French) Lecture Notes in Mathematics, Vol. 323. Springer-Verlag, Berlin-New York, 1973.
[22] J. M. Melenk, *hp-finite element methods for singular perturbations.* Lecture Notes in Mathematics, 1796. Springer-Verlag, Berlin, 2002.
[23] R. E. O'Malley, Singular perturbation analysis for ordinary differential equations. Communications of the Mathematical Institute, Rijksuniversiteit Utrecht, 5. Rijksuniversiteit Utrecht, Mathematical Institute, Utrecht, 1977.
[24] H.-G.Roos, M. Stynes and L. Tobiska, Numerical Methods for Singularly Perturbed Differential Equations. Springer- Verlag, Berlin, 1996.
[25] S. Shih and R. B. Kellogg, *Asymptotic analysis of a singular perturbation problem.* Siam J. Math. Anal. 18(1987), pp 1467-1511.
[26] C. Schwab and M. Suri, The p and hp vesions of the finite element method for problems with boundary layers. Mathematics of Computation. **V. 65** (1996), no. 216, pp. 1403-1429.
[27] M.I. Vishik and L.A. Lyusternik, Regular degeneration and boundary layer for linear differential equations with small parameter, Uspekki Mat. Nauk, **12** (1957), 3-122.
[28] H. K. Versteeg and W. Malalasekera, *An introduction to computational fluid dynamics; the finite volume method.* Pearson Eduction Limited, Glasgow, UK, 2007
[29] R. Temam, *Navier-Stokes equations; theory an numerical analysis*. AMS Chelsea series. AMS, Providence, R.I., 2001.

Ulsan National Institute of Science and Technology, San 194, Banyeon-ri, Eonyang-eup, Uljugun, Ulsan, Republic of Korea.
E-mail: cjung@unist.ac.kr
URL: http://unist.ac.kr/private/changyeoljung

The Institute for Scientific Computing and Applied Mathematics, Indiana University, Bloomington, IN 47405, USA.
E-mail: temam@indiana.edu
URL: http://mypage.iu.edu/∼temam